



Investigation of gamma-(U;Zr) structural properties and its interfacial properties with liquid sodium using ab initio molecular dynamics

August 2022

Changing the World's Energy Future

Ahmed Aly, Maria Avramova, Benjamin W Beeler



DISCLAIMER

This information was prepared as an account of work sponsored by an agency of the U.S. Government. Neither the U.S. Government nor any agency thereof, nor any of their employees, makes any warranty, expressed or implied, or assumes any legal liability or responsibility for the accuracy, completeness, or usefulness, of any information, apparatus, product, or process disclosed, or represents that its use would not infringe privately owned rights. References herein to any specific commercial product, process, or service by trade name, trade mark, manufacturer, or otherwise, does not necessarily constitute or imply its endorsement, recommendation, or favoring by the U.S. Government or any agency thereof. The views and opinions of authors expressed herein do not necessarily state or reflect those of the U.S. Government or any agency thereof.

**Investigation of gamma-(U;Zr) structural properties
and its interfacial properties with liquid sodium using
ab initio molecular dynamics**

Ahmed Aly, Maria Avramova, Benjamin W Beeler

August 2022

**Idaho National Laboratory
Idaho Falls, Idaho 83415**

<http://www.inl.gov>

**Prepared for the
U.S. Department of Energy
Under DOE Idaho Operations Office
Contract DE-AC07-05ID14517**

Investigation of γ -(U, Zr) structural properties and its interfacial properties with liquid sodium using *ab initio* molecular dynamics

Ahmed Aly^a, Benjamin Beeler^{a,b}, Maria Avramova^a

^aNuclear Engineering Department, North Carolina State University, North Carolina, 27695, USA

^bIdaho National Laboratory, Idaho, 83145, USA

Abstract

In this study, the elastic properties, structural parameters, sound velocity, and Debye temperature of γ -(U, Zr) were computed using *ab initio* molecular dynamics (AIMD) at temperatures between 1000 K and 1400 K and for Zr content between 0 *at.*% and 100 *at.*%. UZr is used as a metallic fuel for Sodium Fast Reactors (SFRs). The study of the mechanical and thermal behavior of these alloys leads to a better data-informed fuel design. The bulk modulus, shear modulus, Young's modulus, and Poisson's ratio were calculated from the elastic constants and their dependence on Zr content and temperature was investigated, comparing the results with previous computational work and the available experimental data in the literature. Interfacial properties between UZr (up to 32 *at.*% which typically exists in nuclear fuel) and liquid sodium are also of interest due to the presence of a sodium bond between the fuel and the cladding in metallic nuclear fuel. The interfacial energy between γ -(U, Zr) and liquid sodium, the surface tension of liquid sodium, and the work of adhesion were computed at different temperatures and Zr concentrations. It was demonstrated that γ -(U, Zr) is completely wetted by liquid sodium at all the investigated temperatures and Zr concentrations. This work provides the basis for the determination of interfacial resistances in SFRs and their implementation into heat transfer fuel performance simulations, which will be the subject of future work.

1. Introduction

Uranium alloys are an ideal fuel candidate for sodium-cooled fast reactors (SFRs). Uranium metal (U) is alloyed with zirconium (Zr) to increase the melting point and to stabilize the high temperature body-centered cubic (bcc) phase which improves the irradiation performance of the alloy. The high fissile material density in UZr alloys enables the operation of SFRs at relatively higher power density than traditional light water reactors (LWRs). For

7 this purpose a bond sodium is added between the metallic fuel and the steel-based cladding
8 to enhance the heat transfer properties.

9 The high temperature phases of uranium and zirconium (γU and βZr) have a bcc struc-
10 ture. The γU phase is the stable phase of uranium between 1045 K up to its melting point
11 of 1407 K [1, 2] while βZr phase is between 1140 K up to Zr melting point of 2125 K [3].
12 Due to the similarity of the crystal structure of the high temperature phases of the two
13 metals, U forms substitutional alloys with Zr, which is referred to as $\gamma\text{-(U,Zr)}$. Zr is also
14 compatible with the steel cladding used in SFRs. U-10Zr (10 weight percent) is the standard
15 alloy composition when metallic fuel is considered for SFRs. However, due to constituent
16 redistribution during irradiation in the reactor, the fuel composition varies radially produc-
17 ing regions of depleted zirconium as low as 2 *wt.*% and regions with enriched zirconium as
18 high as 15 *wt.*% [4].

19 The limited experimental data on the $\gamma\text{-(U, Zr)}$ phase has motivated a number of funda-
20 mental computational investigations of its thermophysical properties. Several studies inves-
21 tigated the elastic constants of γU at 0 K using Density Functional Theory (DFT). Taylor
22 [5] investigated α , γ , and face-centered cubic uranium and determined the equilibrium lat-
23 tice parameters and elastic constants for the three structures. Taylor showed that C_{12} was
24 greater than C_{11} in the γ phase, which leads to a negative shear constant $C' = (C_{11} - C_{12})/2$,
25 indicating the instability of the γ phase of uranium at 0 K [6]. Shang et al. [7] used the
26 PW91 Generalized Gradient Approximation (GGA) to calculate, among other properties,
27 the lattice parameters, bulk modulus, and elastic constants of γ phase of uranium (in addi-
28 tion to numerous other elements) at 0 K and their results showed a negative shear constant
29 as well. Several computational studies were performed on βZr using DFT with different
30 exchange correlations [8, 9, 10, 11]. Similar to γU , the instability of this phase at 0 K was
31 confirmed.

32 The low temperature mechanical instabilities yield unrealistic values of the shear modulus
33 and makes the calculation of the Debye temperature and the sound velocities unfeasible. The
34 sound velocities are of interest as they can be incorporated into the acoustic mismatch theory
35 [12, 13] and used in the computation of the interfacial thermal conductance between UZr
36 alloys and the bond material [14]. Knowledge of such interfacial conductance is utilized in
37 fuel performance and thermal transport software. The instability of the γU phase at 0 K
38 and the resultant imaginary sound velocities emphasize the importance of applying *ab initio*
39 molecular dynamics (AIMD) to obtain the UZr properties. The scarcity of experimental
40 data on UZr and the fact that most of these experiments are on un-irradiated U-10Zr alloys
41 primarily before ~ 1970 advocates the importance of the computational work on UZr alloys
42 to provide data on data-sparse regions that need to be further investigated experimentally,

43 in particular the determination of elastic properties [15].

44 There is no previous work in the literature that investigated the interfacial contact prop-
45 erties between UZr alloys and liquid sodium. Aly et al. [16] used AIMD to investigate the
46 surface energy of γ -(U, Zr) for temperatures between 1000 K and 1400 K and Zr concentra-
47 tions from 0 *at.%* to 100 *at.%*. Beeler et al. [17] used classical molecular dynamics (CMD)
48 to investigate the surface energy for the same range of temperatures and compositions. The
49 only available work in the literature that investigated the contact between the uranium metal
50 and the liquid sodium was done by Taylor and Ford [18] in 1955. They used the sessile drop
51 technique to evaluate the contact angle between liquid sodium and several metals and ce-
52 ramics including uranium and uranium dioxide (UO_2) for temperatures up to 825 K. The
53 presence of bonding sodium in contact with the surface of the UZr fuel pins motivated the
54 study of the contact properties between the two metals. At the time of Taylor and Ford,
55 there was not any data available computationally or experimentally for the surface energy
56 of γ -(U, Zr) which made the calculation of the work of adhesion not possible from a simple
57 contact angle relationship.

58 In this work, AIMD was used to determine the bulk modulus, shear modulus, Young's
59 modulus, Poisson's ratio, sound velocity, and Debye temperature for γ -(U, Zr) between 0
60 *wt.%* and 15 *wt.%* along with metallic β Zr for temperatures between 1000 K and 1400 K. The
61 results are compared to the available experimental data and/or previous computational work
62 when available. This study is the first work, to our knowledge, to computationally explore
63 the elastic properties of γ -(U, Zr) and the interfacial properties between liquid sodium and
64 γ -(U, Zr) with *ab initio* methods. Additionally, the surface tension of liquid sodium and the
65 interfacial energy between UZr alloys and liquid sodium were investigated in this work for
66 temperatures between 1000 K and 1400 K. From the results of Aly et al. [16] and the results
67 generated in this work, the work of adhesion and the contact angle were evaluated.

68 2. Computational details

69 The Vienna *ab initio* Simulation Package (VASP) was utilized for all the performed calcu-
70 lations [19, 20]. The Projector augmented wave (PAW) method was utilized within the DFT
71 framework [21]. The calculations were performed using the Perdew-Burke-Ernzerhof (PBE)
72 GGA density functional implementation for the description of the exchange-correlation [22].
73 For uranium, a PAW pseudopotential with fourteen valence electrons and a core represented
74 by [Xe,5d,4f] was utilized. For zirconium, the pseudopotential contained twelve valence elec-
75 trons while the core was defined by [Ar,4d]. The supercell size was 4x4x4 bcc structured unit
76 cells. A gamma-centered Monkhorst-Pack [23] 1x1x1 k-point mesh was used for Brillouin
77 zone sampling. Uranium is assumed to be non-magnetic, in accordance with experiments

78 and previous simulations [24], hence, the calculations are non-spin polarized. The energy
79 cutoff was taken to be 300 eV, which is approximately 50 eV higher than the maximum sug-
80 gested energy cutoff from the pseudopotential of uranium. The electronic self-consistent loop
81 convergence criterion is taken to be 10^{-4} . The Nosé-Hoover thermostat is used to control
82 the system temperature. The SMASS parameter which controls the velocities during AIMD
83 calculations was zero which means that a Nosé-mass corresponding to a period of 40 time
84 steps will be chosen. The timestep was taken to be 2.0 fs. The Hubbard U parameter is not
85 utilized in this work, as it has been shown that it is not necessary for the accurate description
86 of metallic uranium [5, 6, 25]. For the purpose of this paper, spin-orbit coupling (SOC) is
87 not considered for the analysis of the UZr alloys. Generally, SOC should not be neglected for
88 actinides, but proper implementation of SOC should be investigated and established prior
89 to its full utilization [26].

90 The simulations were performed for a temperature range between 1000 K and 1400 K.
91 The Zr concentration ranged between 0 *at.%* to 100 *at.%*. The alloy compositions in be-
92 tween these values were generated by substituting a specified number of uranium atoms with
93 Zr atoms at random locations within the lattice. This was confirmed by checking the pair
94 distribution function of the generated atomic configuration using OVITO V.3.3.4 [27]. The
95 simulations were performed using three unique random UZr configurations for each compo-
96 sition to gain statistical significance of the results and ensure that the results obtained were
97 not configuration-dependant.

98 *2.1. Calculation of Interfacial Energies*

99 The calculations of the interfacial energies between the sodium coolant and the UZr
100 system were performed in two steps: (1) calculations involving only either liquid sodium or
101 bulk UZr; (2) calculations involving a system with bulk UZr alloy in contact with liquid
102 sodium.

103 In step one, the properties of sodium were investigated for a system of 686 atoms con-
104 sisting of 7x7x7 bcc unit cells. A single gamma point sampling was used to model the
105 Brillouin zone. Initially, the lattice parameter of the bcc sodium at 293 K was determined
106 by performing five NVT simulations at various values of lattice parameters. The system
107 pressure is obtained at each case and the equilibrium lattice parameter is determined as
108 the lattice parameter at which the average pressure of the system is zero. The obtained
109 lattice parameter for bcc sodium at room temperature was 4.28 Å. This value is consistent
110 with the known lattice parameter of sodium at room temperature of 4.29 Å [28, 29]. The
111 production simulations began with a 10 ps relaxation at 293 K where an ideal bcc sodium
112 is allowed to thermalize at room temperature. The approach followed afterwards is the *melt*

113 *and quench* approach. In this technique, the sodium temperature is increased to a theoret-
114 cal temperature of 4000 K. The system is simulated at this temperature for 15 ps which is
115 sufficient to ensure the breaking of all the bonds between the solid sodium atoms, turning
116 it to a liquid [30]. The temperature is then decreased in increments of 500 K and the sys-
117 tem is equilibrated for a period of 10 ps at each temperature to ensure the removal of any
118 effect of the previous temperature. The system pressure and energy were examined after
119 each stage to ensure that the system had reached a stable behavior before advancing to the
120 next temperature. The process continued until the system reaches the investigated working
121 temperatures between 1000 K and 1400 K where the system is further equilibrated for 10
122 ps. Finally the systems were simulated in an NPT ensemble allowing the system volume to
123 change to equilibrate the system pressure to zero. Once the average pressure is stabilized
124 around zero, the system volume is measured over the course of 10 ps to obtain an average
125 system volume from which the liquid sodium density was calculated, as well as the sodium
126 energy per atom at the temperature range of interest.

127 The equilibrium volume of γ -(U, Zr) was previously determined [16] and a system con-
128 taining only the solid UZr was simulated in an NVT ensemble at the equilibrium volumes
129 for different temperatures and concentrations of Zr. The purpose of these simulations was
130 to determine the energy of the bulk UZr system. The simulations were evolved for 10 ps,
131 where the first 5 ps served to equilibrate the system, and the second 5 ps were utilized to
132 determine the system energy. During the simulations, the pressure was monitored to ensure
133 that the system is stable at the prescribed equilibrium volumes.

134 The second step of the simulation involved a combination of two phases of equal volume in
135 contact with each other. The first phase is the UZr solid system with atomic concentrations
136 between 0 *at.%* and 32 *at.%* Zr, and the second phase is a configuration of liquid sodium.
137 Based on the liquid sodium density determined in the first phase, the number of liquid sodium
138 atoms that can fill the volume designated for the coolant was determined to be between 50
139 to 58 atoms for temperatures between 1000 K to 1400 K, respectively. A second set of
140 sodium-only simulations were performed in an NVT ensemble at the prescribed two-phase
141 sodium volume. The purpose of this task was to generate a variety of random configurations
142 of sodium in the liquid phase at the temperature range of interest that can be combined
143 with the bulk UZr, ensuring no effects of the initial sodium structure. Subsequently, the
144 two-phase supercells were constructed.

145 The UZr/Na system is equilibrated in an NPT ensemble for 4 ps to ensure that the sys-
146 tem is equilibrated and the pressure is averaged to zero before performing the production
147 simulations. After equilibrating the UZr/Na systems, simulations were evolved for 15 ps in
148 an NPT ensemble to ensure that the energy of the system is stable and oscillating around

149 an average value. The last 5 ps of these simulations are used to obtain an average potential
 150 energy value of the UZr/Na system. The interfacial energy per unit area between the UZr
 151 metal fuel and the sodium coolant is determined using the following equation:

$$152 \quad E_{Interface} = \frac{E(UZr/Na) - E(UZr) - E(Na)}{2A_{Interface}} \quad (1)$$

153 where $E(UZr)$ is the energy of the solid UZr bulk, $E(Na)$ is energy of the liquid sodium
 154 bulk, $E(UZr/Na)$ is the energy of the combined two-phase system, and $A_{Interface}$ is the area
 155 of the interface. Due to the simulation geometry, two identical interfaces are generated.
 156

157 To calculate the surface tension (γ_{Na}) of liquid sodium, a supercell containing 686 sodium
 158 atoms was thermalized to obtain seven random liquid sodium configurations at each temper-
 159 ature of interest using the *melt and quench* technique. The size of the supercell was chosen
 160 based on the calculated sodium density as a function of temperature. The production simu-
 161 lations were based on systems of size LxLxL to obtain the bulk sodium energy. Afterwards,
 162 a surface is added by modeling a system of size LxLx2L in which sodium comes in contact
 163 with a vacuum region as shown in figure 1. The surface tension of liquid sodium (γ_{Na}) is
 164 calculated from equation 2

$$\gamma_{Na} = \frac{E^* - E}{2A} \times N \quad (2)$$

165 where E^* and E are the energy per atom with a surface and the bulk sodium energy, respec-
 166 tively, N is the number of atoms in the system, A is the surface area, and there exist two
 167 surfaces in the system due to periodic boundaries, hence the division by 2.

168 The work of adhesion (W_{SL}) is calculated from the Dupré equation [31] which can be
 169 expressed for solids in contact with a liquid on the form of equation 3.

$$W_{SL} = \gamma_{UZr} + \gamma_{Na} - E_{Interface} \quad (3)$$

170 where γ_{UZr} is the surface energy of UZr [16].

171 The contact angle (θ) between a solid and a liquid can be calculated from the Young-
 172 Dupré equation [31] which can be written as follows

$$W_{SL} = \gamma_{Na}(\cos\theta + 1) \quad (4)$$

173 From equations 3 and 4, the condition for which complete spreading of the liquid on a solid
 174 surface i.e ($\cos\theta \geq 1$) can be expressed as

$$\gamma_{Na} + E_{Interface} - \gamma_{UZr} \leq 0 \quad (5)$$

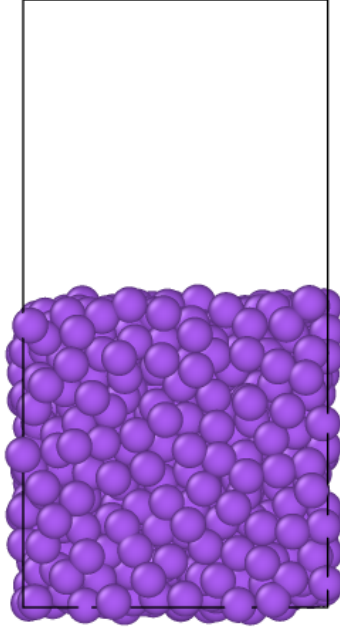


Figure 1: Random structure of liquid sodium of a system containing 686 atoms with dimensions $L \times L \times 2L$ used in calculating the surface energy at 1000 K.

175 *2.2. Calculation of Elastic Properties*

176 The Voigt-Reuss-Hill [32] scheme was used to determine the bulk and shear effective
 177 moduli for a polycrystalline system as the arithmetic mean of the two bounds for mono-
 178 crystals according to Voigt [33] and Reuss and Agnew [34]. This approach was used in a
 179 number of diverse studies to determine these properties [35, 36, 37]. As previously explained,
 180 the equilibrated system at zero pressure was simulated. The next step was to apply a small
 181 strain of 1.0 % to determine the elastic constants of UZr (C_{ij}).

182 The production simulations involved three random UZr configurations with ten initial
 183 velocity distributions for each configuration leading to a total of thirty production simulations
 184 at each temperature and Zr concentration to ensure statistical significance of the obtained
 185 results. The elongation stresses and elastic constants for longitudinal expansion (C_{11} , C_{22} and
 186 C_{33}), the transverse expansion elastic constants (C_{12} , C_{23} and C_{31}), and the shear moduli
 187 (C_{44} , C_{55} , and C_{66}) are all of interest in this work. Because of the symmetry of the bcc
 188 structure of UZr, the problem reduces as C_{11} , C_{22} and C_{33} are equal, and C_{12} , C_{23} and C_{31}
 189 are equal, and C_{44} , C_{55} and C_{66} are equal, yielding only three independent elastic constants.

190 The elastic constants are obtained by solving linear stresses versus strain equations. From
 191 these constants, the bulk modulus (B), shear modulus (G), Young's modulus (E), and Pois-
 192 son's ratio (ν) [35] are obtained from the following set of equations:

193

$$B = \frac{1}{9}(3C_{11} + 6C_{22}) \quad (6)$$

$$G = \frac{1}{2} \left[\frac{C_{11} - C_{12} + 3C_{44}}{5} + \frac{5C_{44}(C_{11} - C_{12})}{4C_{44} + 3(C_{11} - C_{12})} \right] \quad (7)$$

$$E = \frac{9BG}{3B + G} \quad (8)$$

$$\nu = \frac{3B - E}{6B} \quad (9)$$

194

195 The longitudinal and transverse sound velocities [38] were computed from the following
196 equations:

$$v_l = \left(\frac{3B + 4G}{3\rho} \right)^{1/2} \quad (10)$$

$$v_t = \left(\frac{G}{\rho} \right)^{1/2} \quad (11)$$

197 where v_l and v_t are the longitudinal and transverse sound velocities in an isotropic material,
198 respectively. The mean sound velocity [38] can be calculated by:

$$v_m = \frac{1}{3} \left(\frac{2}{v_t^3} + \frac{1}{v_l^3} \right)^{-1/3} \quad (12)$$

199 The Debye temperature (θ_D) [38] can be estimated from the mean sound velocity as follows:

$$\theta_D = \frac{h}{K_B} \left[\frac{3}{4\pi V_a} \right]^{1/3} v_m \quad (13)$$

200 The error of the mean in the properties computed in this work were computed and
201 propagated through the equations to obtain the uncertainty level in the computed data
202 properties. The estimation of the error began by computing the mean error of the elastic
203 constants, as determined from equation 14

$$SE = \frac{SD}{\sqrt{N}} \quad (14)$$

204 where SE and SD is the standard error and standard deviation, respectively. N is the
205 number of simulations performed to obtain the mean value of the elastic constants. The

206 errors are then propagated through the equations based on equations 15, 16 and 17 for
207 addition/subtraction, multiplication/division, and powers, respectively [39]:

$$\delta Q = \sqrt{(\delta a)^2 + (\delta b)^2} \quad (15)$$

208 in the case where $Q = a + b$,

$$\frac{\delta Q}{|Q|} = \sqrt{\left(\frac{(\delta a)}{|a|}\right)^2 + \left(\frac{(\delta b)}{|b|}\right)^2} \quad (16)$$

209 in the case where $Q = a \times b$, and

$$\frac{\delta Q}{|Q|} = n \frac{\delta x}{|x|} \quad (17)$$

210 in the case where $Q = x^n$.

211 **3. Results and discussion**

212 *3.1. Interfacial energy between solid UZr and liquid Na*

213 The sodium density was calculated as a function of temperature. The results are plotted
214 in figure 2 and compared to the experimental data reported in Leibowitz et al. [40, 41]. The
215 obtained results are slightly over-predicted relative to the experimental data. Nevertheless,
216 the error in our data contains the experimental values. It should be noted as well that the
217 points on the experimental data curve for 1300 K and 1400 K are extrapolated from the
218 reported experimental data for comparison purposes. Due to the good agreement of the
219 density of sodium predicted from AIMD with experimental results, the computed densities
220 were used to construct a bulk sample of liquid sodium that was connected to the UZr bulk
221 to calculate the interfacial energies.

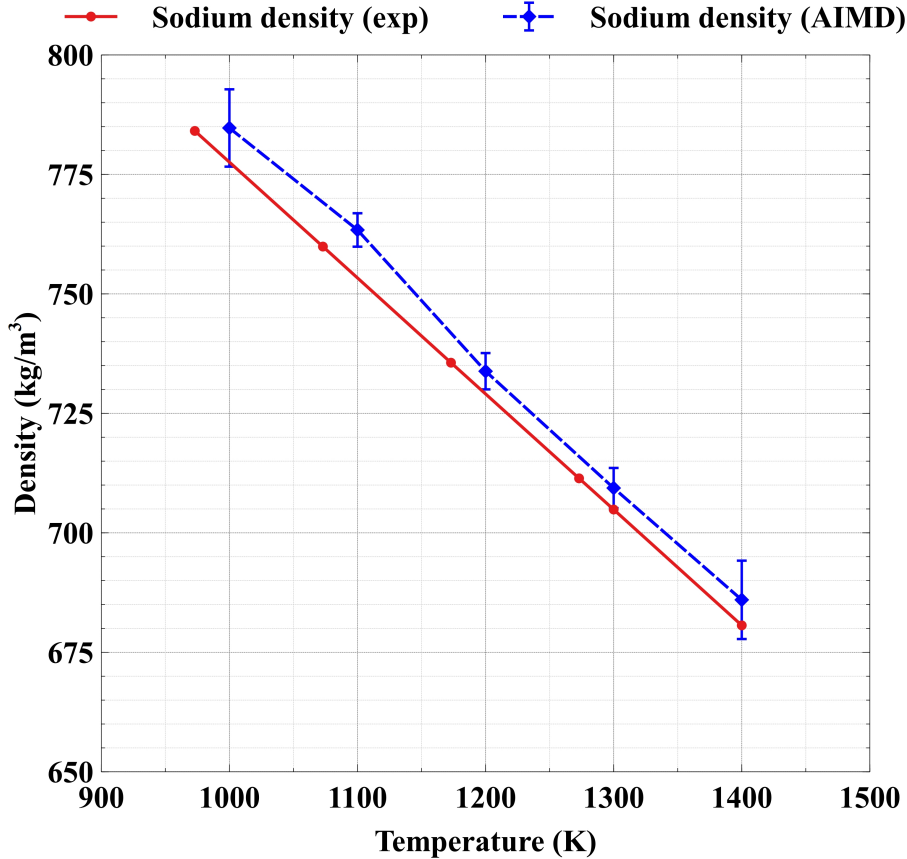


Figure 2: Sodium density from experimental data [40] [41] and the predictions from AIMD calculations.

222 The surface tension of liquid sodium γ_{Na} was evaluated from the computational data using
 223 equation 2. The value of surface tension is found to be almost constant ($\approx 182 \text{ mN/m} \pm 8$
 224 mN/m) with temperature in the range between 1000 K and 1400. This value is comparable
 225 to the value of surface tension determined experimentally for liquid sodium at temperature
 226 around its melting point of 371 K which was 194 mN/m [42]. However, the computed value
 227 is over-predicted when compared to the value expected based on the analysis of Goldman [43]
 228 of the available experimental data and their fitting to the Van der Waals equation [44] which
 229 was 132 mN/m . This over-prediction might be due to the small size of simulated system of
 230 686, or the usage of a single Γ point in this work [45], however, such approximations have
 231 been sufficient for prior liquid system analyses [46, 47, 48]. Additional increases in system
 232 size or increase in density of k points will likely lead to excessive computational expenses
 233 rendering this type of work unfeasible. The surface tension of sodium is relatively lower than
 234 most of other liquid metals at their melting temperature [49] with the exception of cesium (68
 235 mN/m), rubidium (81 mN/m), and potassium (110 mN/m) which makes sodium wetting
 236 solid surfaces much easier than mercury, which has a surface tension value of 500 mN/m .

237 Figure 3 depicts the contact and interface between the two systems for a U-10Zr system at
 238 1000 K as a representation of how our systems are constructed for various Zr concentrations
 239 and temperatures. It should be emphasized that all boundaries are periodic, and thus there
 240 is one interface in the center of the supercell, and a second interface on the top/bottom of
 241 the supercell in Figure 3. Figure 4 depicts the predicted interfacial energies for UZr-Na as a
 242 function of Zr concentration up to 32 *at.%* Zr. It can be noticed that the interfacial energy
 243 slightly decreases with the increase of the Zr content but remains within the range of 1 to
 244 1.3 J/m². The error in the mean values of the interfacial energies falls between 0.02 to 0.035
 245 J/m². An increase in temperature leads to a corresponding increase in the interfacial energy.
 246 This is consistent with the increase in surface energy observed for the UZr surfaces without
 247 sodium [16]. It should be mentioned that the surface energy of γ -(U, Zr) decreases with the
 248 increase of Zr content. This change is steeper at higher temperature and more gradual as
 249 the temperature decreases farther away from the solidus temperature of the alloy [16].

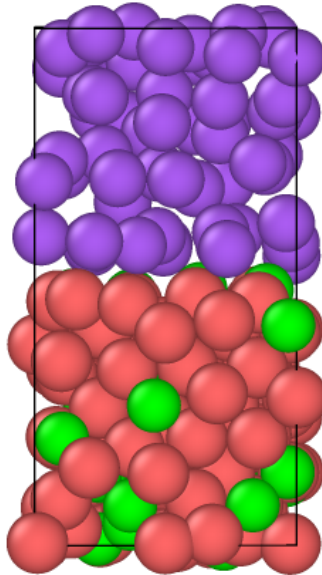


Figure 3: Schematic of the γ -(U,10Zr) interface with liquid sodium, the red, green and purple spheres represents uranium, zirconium and sodium atoms respectively.

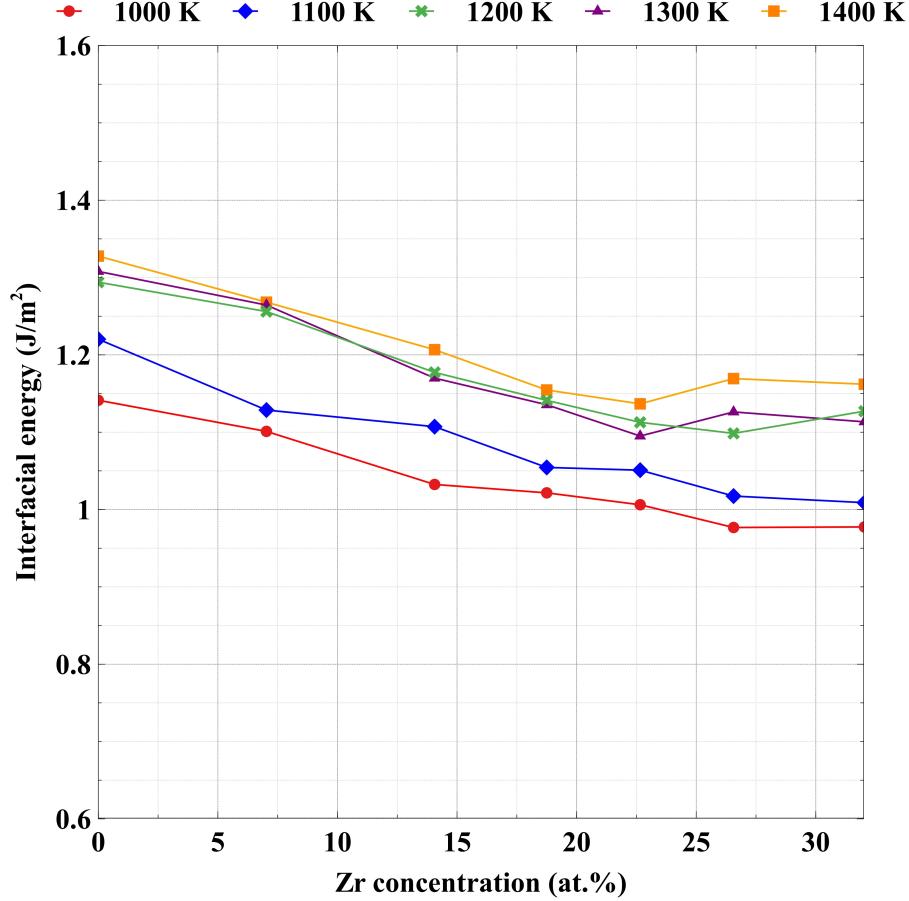


Figure 4: The interfacial energy between UZr and sodium as a function of Zr content between 1000 K and 1400 K .

250 The work of adhesion was calculated from equation 3 and is plotted in figure 5. It can be
 251 noticed that the work of adhesion values for low Zr content systems do not vary drastically
 252 with temperature below 1300 K, but there is a rapid change going to 1400 K. This behavior
 253 follows that of the surface energy of $\gamma-(U, Zr)$ which, at low Zr concentrations, has a rapid
 254 change in the surface energy above 1300 K which might be attributed to the closeness of
 255 temperature above this value to the solidus temperature of the alloy. With the increase of
 256 the Zr content, the melting temperature increases and the variation of the surface energy
 257 with temperature decreases, which is what is noticed in figure 5 for the work of adhesion as
 258 well. It should also be mentioned that the difference between the computed sodium surface
 259 tension and the experimental values, 0.05 J/m^2 , has a maximum effect on the computed
 260 work of adhesion of about 8% for metallic U at 1000 k which is close to the uncertainty limit
 261 of the predicted work of adhesion which lies between 0.03 and 0.04 J/m^2 .

262 The contact angle (θ) between $\gamma-(U, Zr)$ and liquid sodium was investigated by first
 263 checking the complete wettability condition using equation 5. The condition $\gamma_{Na} + E_{Interface} -$

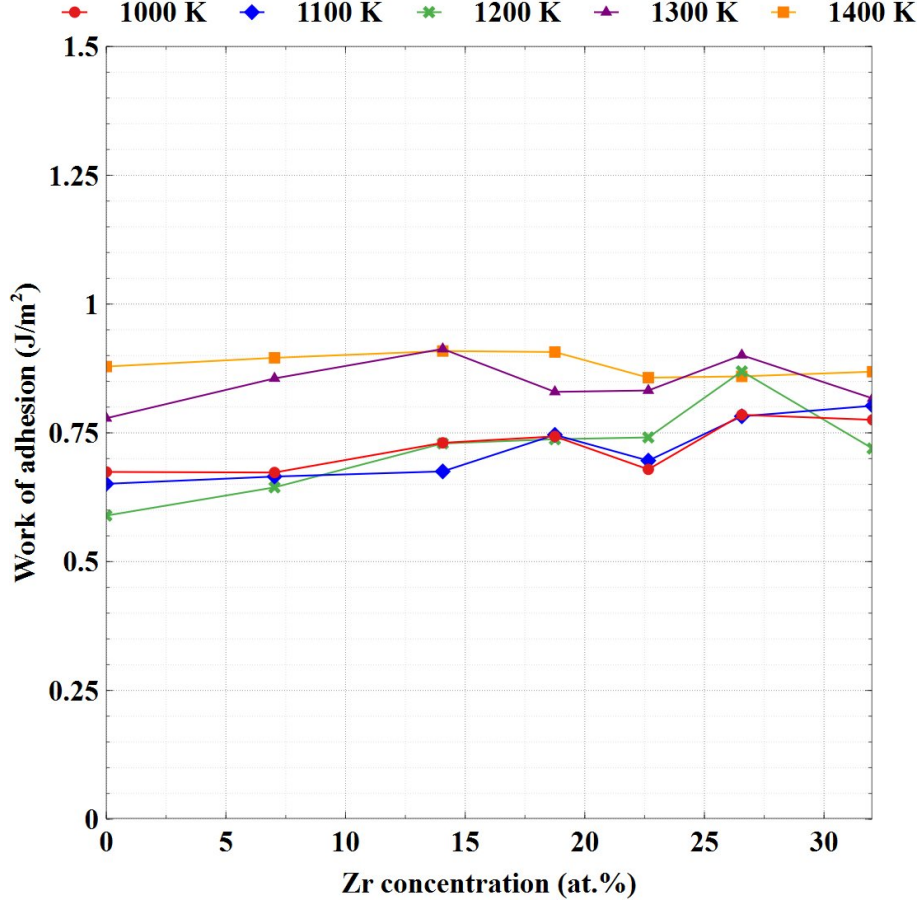


Figure 5: The work of adhesion of $\gamma_-(U, Zr)$ as a function of temperature and Zr concentration.

264 γ_{UZr} was met for all concentrations of Zr at all temperatures. Since a complete spread of the
 265 sodium on $\gamma_-(U, Zr)$ was expected, there was no need to compute the contact angle using
 266 equation 4 since it will give a value of $\cos(\theta) > 1$ which is meaningless. The relatively low
 267 surface tension of sodium makes its wetting of solid surfaces much easier. This is a great
 268 characteristic that enhances the heat transfer when sodium is used as a bonding material or
 269 a coolant in metallic fueled SFRs. This result follows the trend of the data from Taylor and
 270 Ford [18] where they noticed a steep decrease in the contact angle between liquid sodium
 271 and uranium for temperatures above 600 K. The contact angle decreased linearly from 50°
 272 at 773 K to 32° at 823 K which indicates, if extrapolated, that the contact angle reaches
 273 zero directly below 1000 K.

274 This is the first computational work performed to investigate the interfacial characteristics
 275 between $\gamma_-(U, Zr)$ and sodium. The only experimental work in the literature was performed
 276 to compute the contact angle between sodium and various metals including uranium in 1955
 277 [18] using the sessile drop technique. Hodkin et al. [50] used the same technique to determine
 278 the interfacial free energy of UC to be 0.73 J/m^2 and the interfacial energy for solid U-UC

279 system to be 0.141 J/m². Hu et al. [51] used molecular dynamics to determine the surface
 280 energy between solid/liquid U to be 0.077 J/m². The interfacial energy predicted in this
 281 work for U-10Zr at 1000 K was about 1 J/m². There were no data of UZr alloys in contact
 282 with a different liquid metal to compare our results to them. No experimental work can be
 283 directly compared to the present research.

284 3.2. Structural parameters and elastic constant of γ -(U, Zr)

285 The optimized lattice parameters of γ -(U, Zr) are summarized in table A.1 as a function
 286 of temperature and Zr content and the elastic constants are summarized in table A.2 in
 287 Appendix A. For illustration purposes the elastic constants C_{11} , C_{12} , and C_{44} are plotted in
 288 figure 6 for γ U, U-10Zr, and β Zr as a function of temperature. In figure 6 we can notice that
 289 C_{11} is always greater than C_{12} for the pure metals and the U-10Zr alloys. Previous work
 290 performed at 0 K for γ U has predicted negative shear constants, $C' = (C_{11}-C_{12})/2$, which
 291 indicated the instability of the γ phase at 0 K [6, 2]. This made the determination of some
 292 of the mechanical properties mentioned in their work not possible. As evidenced in table
 293 A.2 and figure 6, shear constants are positive in this work which emphasizes the advantage
 294 of using AIMD in the determination of the elastic properties of γ -(U, Zr) at temperatures
 295 higher than 0 K, specifically, at the practical temperatures in which this phase exists between
 296 1045 K to 1480 K (depending on the concentration of Zr). The error of the mean of the
 297 elastic constants varies between 2 and 3.5 GPa for low Zr content and decreases with the
 298 increase of the Zr content to values between 1 and 2.5 GPa for β Zr.

299 The elastic constants obtained in this work were compared to some of the data available
 300 in the literature for γ U. The C_{11} values obtained for γ U (\approx 115 GPa) in this work are
 301 comparable to previous computational work using MD by Moore et al. [52] where they
 302 predicted a value of 111 GPa. The C_{44} values (\approx 50 GPa) are comparable to the results
 303 obtained by Moore et al. [53] using MD and Li et al. [54] using 0 K DFT. However, when the
 304 C_{12} values (\approx 97 GPa) are compared to results using DFT, the values don't compare because
 305 of the negative shear modulus and the high values of C_{12} predicted at 0 K. The results for
 306 C_{11} (\approx 83.5 GPa) for β Zr are consistent with the computational results from Ikehata et al.
 307 [10] (84.2 GPa) and Wang et al. [8] (86.6 GPa) using DFT. For UZr systems, there was no
 308 computational work available for comparison. Additionally, there is no experimental work
 309 available for comparison of the elastic constants.

310 The bulk modulus is determined using equation 6 for γ -(U, Zr) and is plotted in figure 7.
 311 Error bars are only included at 1200 K for readability of figure 7. The results for γ U (\approx 105
 312 GPa) are slightly under-predicted but generally consistent with the bulk modulus determined
 313 by Yoo et al. [55] (113 GPa) who fitted a temperature-independent equation of state (which

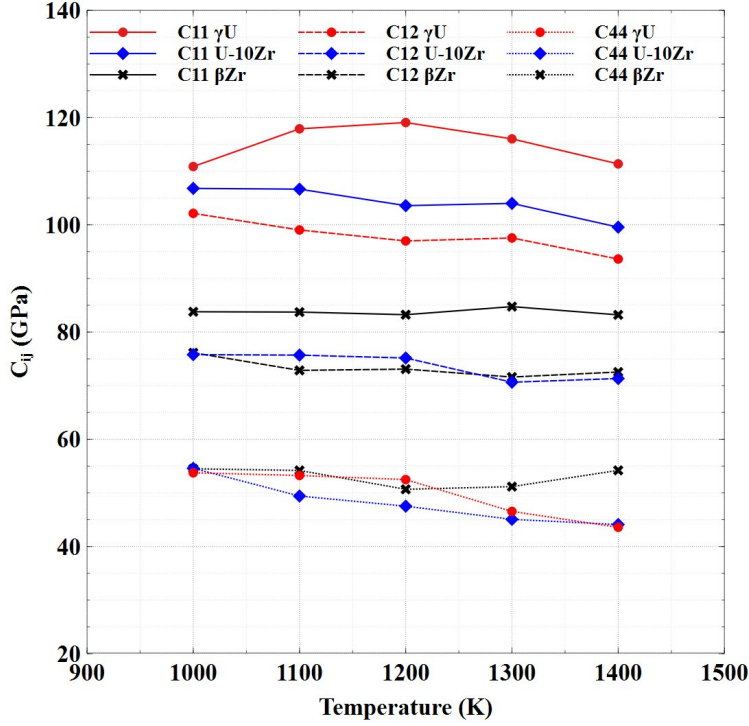


Figure 6: C_{ij} as a function of temperature for γU (red circles), U-10Zr (black crosses), and βZr (blue diamonds).

314 is the only available experimental data for comparison). The bulk modulus values for βZr
315 (≈ 76.5 GPa) are slightly over-predicted when compared to the values obtained by Zhao et
316 al. [56] (66 GPa at 975 K). However, the lattice parameter obtained by their study at 975
317 K was 3.627 \AA , which is higher than the value used in this work at 1000 K (3.61 \AA). The
318 bulk modulus generally softens with increasing temperature, as is expected. The results are
319 under-predicted when compared with previous calculations of the bulk modulus [16] through
320 a different method, but still within the uncertainty limits of the predicted values.

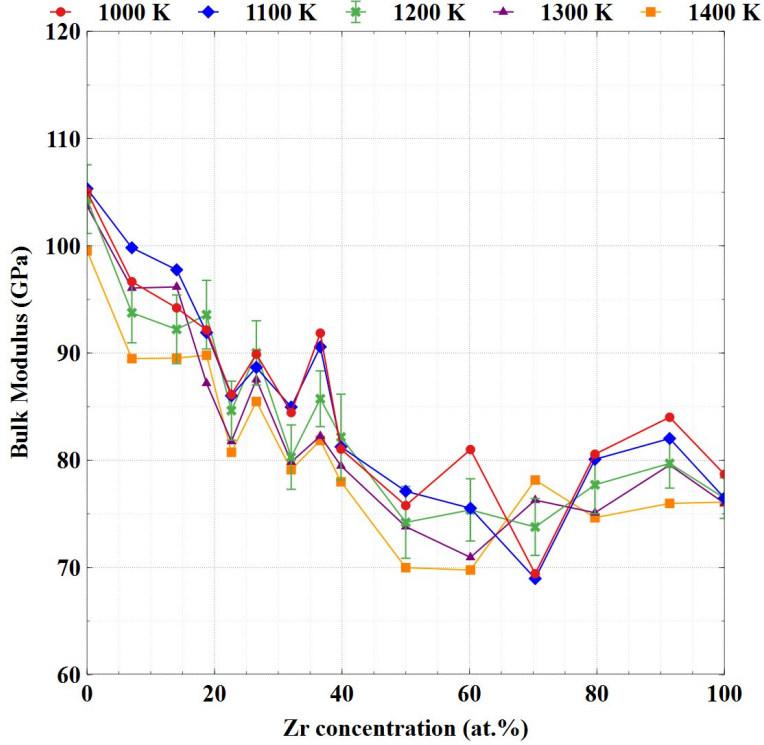


Figure 7: The bulk Modulus of UZr as a function of temperature and Zr concentration as predicted using the elastic constants.

321 The shear and Young's moduli are plotted in figure 8 and the Poisson's ratio is plotted
 322 in figure 9. Error bars are only included at 1200 K for readability of the figures. There is
 323 no clear pattern of temperature dependency of the mentioned elastic properties. The error
 324 of the mean for the shear modulus is about 4 GPa and that for Young's modulus is about
 325 10 GPa as shown in figure 8 for the data at 1200 K. It can be noticed how the error bars at
 326 1200 K overlap with the rest of the data points. Within these uncertainty limits, the data
 327 seems to oscillate without either a clear increase or decrease with temperature which does
 328 not make the resolving of a temperature dependence pattern possible. As for the Zr content,
 329 both moduli increase as a function of Zr content up to ≈ 40 at.% then seems to decrease
 330 almost linearly down to 22 GPa and 62 GPa for the shear modulus and Young's modulus,
 331 respectively, for β Zr

332 For Poisson's ratio (figure 9), the same issue related to the temperature dependence can
 333 be observed. The error in the mean values was about 0.022 which covers the investigated
 334 range of temperature as shown in figure 9. No clear pattern of temperature dependence can
 335 be noticed and the level of uncertainty in the data does not make resolving the temperature
 336 dependence possible at this level of confidence. The Poisson's ratio seems to be decreasing
 337 with Zr content down around 0.3 at 50 at.% then begins to increase to ≈ 0.36 for β Zr

338 The obtained results were compared to the shear and Young's moduli experimental data
 339 obtained from Armstrong et al. for γ U [57]. They measured a Young's modulus value of
 340 24 GPa at 1100 K. They did not report the shear modulus for γ U. However, they included
 341 experimental data point from Holden [58] where the shear modulus was measured to be
 342 about 14 GPa at 1075 K which is close to our predicted value at 1000 K of 21 GPa.

343 Keene et al. [59] determined the dynamic Young's modulus, shear modulus, and Poisson's
 344 ratio as a function of temperature for depleted uranium alloyed with 0.75 *wt.*% titanium.
 345 Their measured value of Young's modulus for γ U was between 99.7 and 99 GPa for tempera-
 346 tures between 1000 K and 1125 K, respectively. The Young's modulus computed in this work
 347 for the same temperature range varied between 62 GPa and 75 GPa which is under-predicted
 348 relative to their data. However, an aspect of the intent of alloying with Ti is to improve
 349 the mechanical properties of metallic U. The measured shear modulus and the calculated
 350 Poisson's ratio in the same temperature range were 35 GPa and 0.41, respectively, which are
 351 close to our predictions for γ U, at the same temperature range, of 27 GPa and 0.4. There
 352 were no experimental data available for β Zr to compare with our results.

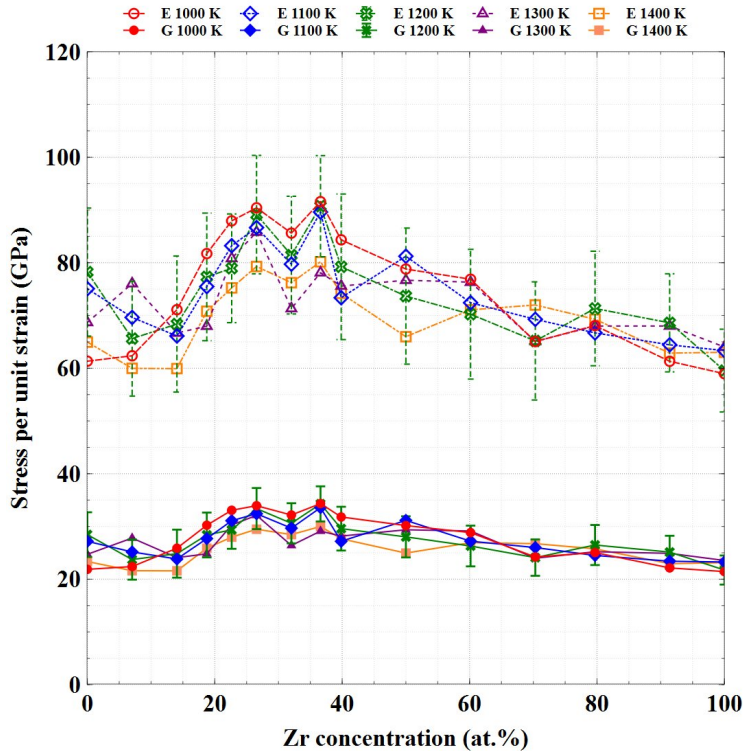


Figure 8: The shear modulus (solid markers) and Young's modulus (Hollow markers) of UZr as a function of temperature and Zr concentration as predicted using the elastic constants.

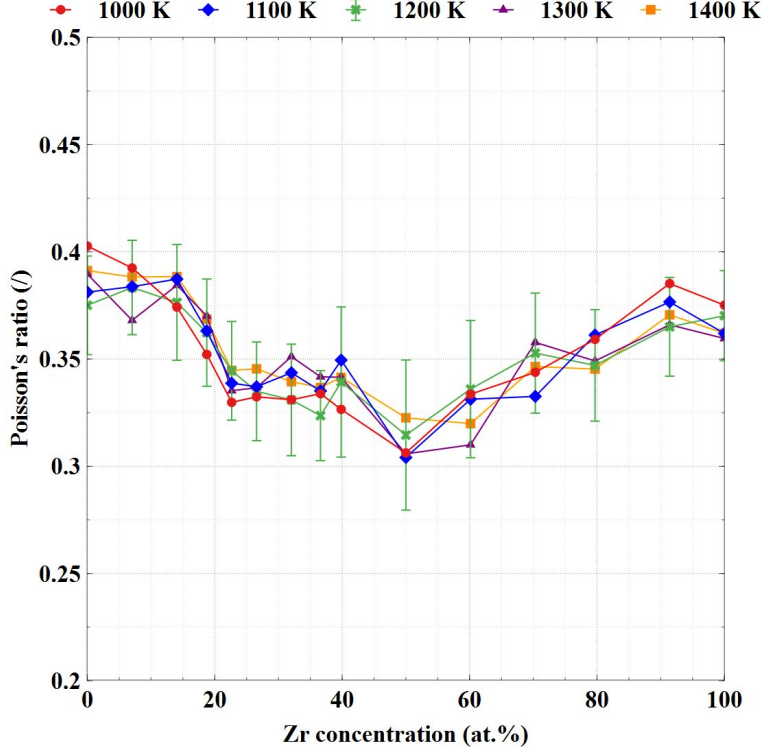


Figure 9: Poisson's ratio of UZr as a function of temperature and Zr concentration.

3.3. Sound velocity & Debye temperature

The longitudinal, transverse, and mean sound velocity in UZr alloys were determined from equations 10 through 12. The sound velocity in UZr showed a weak dependence on the temperature. The sound velocity increased about 100 m/s between 1000 K and 1400 K. The error of the mean in the computed data varied between 80 m/s and 120 m/s. The speed of sound increased with the Zr content on the alloy and can be assumed to be a function of Zr content only.

The temperature-independent longitudinal, transverse, and mean sound velocity are plotted in figure 10 as a function of Zr content. The figure illustrates the increasing trend of the sound velocity with zirconium content. It can be noticed that the mean sound velocity is closer to the transverse velocity than the longitudinal one, which is expected as there are two transverse propagation directions compared to the single longitudinal directional component.

The sound velocity was fitted to the following equations and are plotted in figure 10 as well.

$$V_L(Zr) = 1.506^{-3}Zr^3 - 0.0828Zr^2 + 7.92Zr + 2691 \quad (18)$$

$$V_t(Zr) = 9.9^{-4}Zr^3 - 0.17Zr^2 + 14.778Zr + 1110 \quad (19)$$

$$V_m(Zr) = 1.11^{-3}Zr^3 - 0.185Zr^2 + 16.054Zr + 1257 \quad (20)$$

371 The Debye temperature is plotted in figure 11 where it can be noticed as the Zr content
 372 increases, so does the Debye temperature. The Debye temperature does not strongly vary
 373 with the temperature, and the reported data has an error margin between 9 and 14 K,
 374 as can be noticed in figure 11 for 1200 K. Error bars are only included at 1200 K for
 375 readability of figure 11. Thus, the temperature dependence of the Debye temperature cannot
 376 be established. Due to the small variation with temperature, it can be assumed that the
 377 Debye temperature is temperature-independent in this temperature range and varies between
 378 130 K and 225 K for γ U and β Zr, respectively.

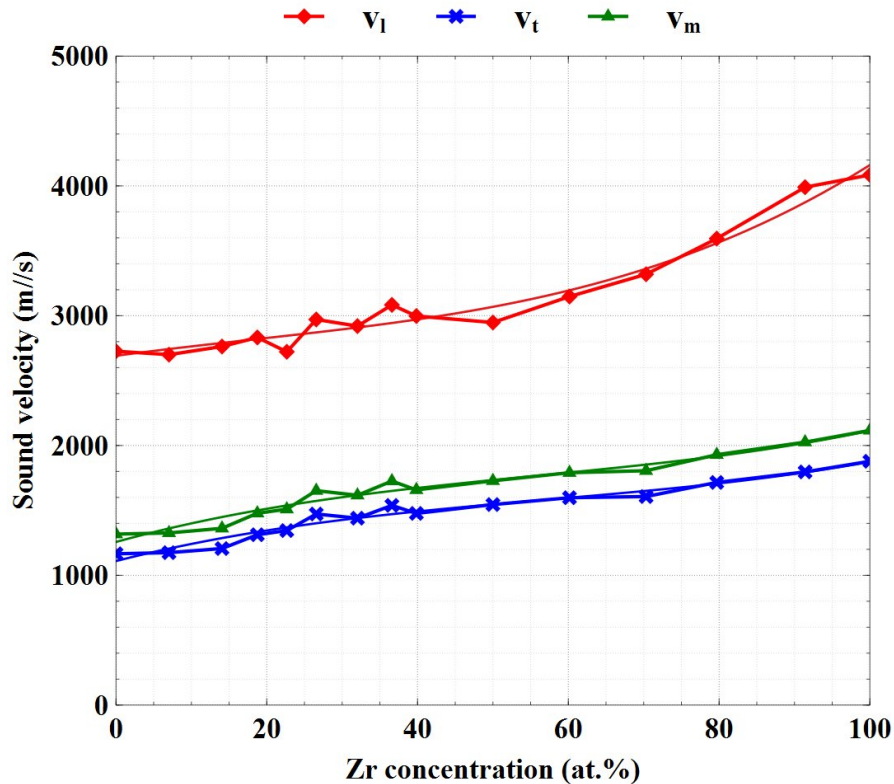


Figure 10: The temperature-averaged longitudinal, transverse and mean Sound velocity as function of Zr content.

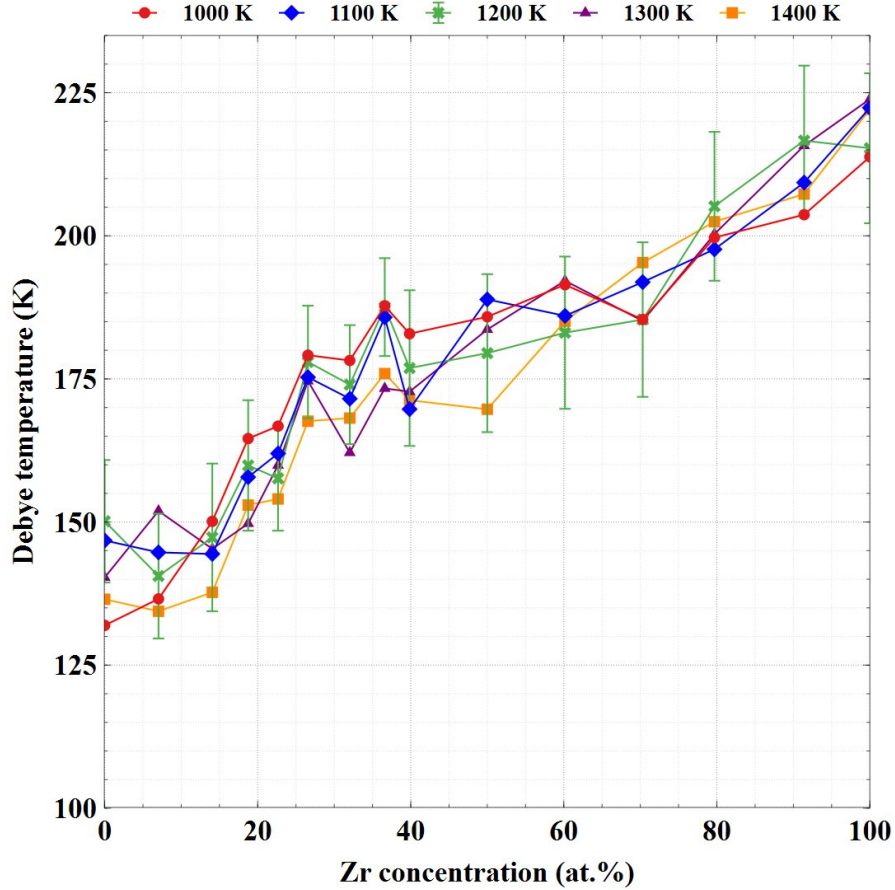


Figure 11: The Debye temperature as a function of temperature and Zr content

379 4. Conclusions

380 In this work, AIMD was used to determine the interfacial energy between $\gamma-(U, Zr)$ and
 381 liquid sodium with Zr concentrations up to 32 *at.%*. Elastic constants, structural properties,
 382 sound velocity, and the Debye temperature of $\gamma-(U, Zr)$ were computed for the alloys between
 383 0 *at.%* and 100 *at.%* Zr. The interfacial energy between UZr and liquid sodium was found
 384 to decrease with Zr content up to 25 *at.%* Zr, after which, there was no noticeable decrease
 385 in the interfacial energy with Zr content. The interfacial energy tends to increase with
 386 temperature but this increase slows down for temperatures between 1200 K and 1400 K,
 387 which might be related to the vicinity of these temperatures to the melting point of UZr
 388 alloys. The surface tension of sodium was computed in this work, however the obtained
 389 value of 185 *mN/m* is over-predicting the experimental data by ≈ 50 *mN/m*. Nevertheless,
 390 the relatively low surface tension of liquid sodium makes any errors from the computation
 391 data insignificant when used to compute the work of adhesion.

392 The work of adhesion was computed from the surface energy of $\gamma-(U, Zr)$, the surface

393 tension of sodium, and the interfacial energy between UZr and the liquid sodium. The
394 obtained results follow the same pattern of $\gamma(U, Zr)$ surface energy in which the temperature
395 dependence decreases with the increase of Zr content in the alloy. It was shown that the
396 liquid sodium completely spreads on the surface of $\gamma(U, Zr)$ which enhances the heat transfer
397 properties between this phase in the metallic fuel and the bonding sodium. This information
398 can be incorporated into mesoscale and engineering scale models which utilize surface and
399 interfacial energies to describe phenomena such as porosity formation, fission gas bubble
400 swelling, and wetting.

401 The elastic constants were computed for $\gamma(U, Zr)$. The C_{11} and C_{44} were comparable
402 to several other studies using MD or DFT at 0 K. There was no basis for comparison of
403 C_{12} since the available data at 0 K leads to negative shear constant values. The bulk
404 modulus was calculated based on the lattice constant data and the results are consistent
405 but slightly under-predicted when compared to our previous work [16] and slightly under-
406 predicting the only available experimental data for γ U by Yoo et al. [55]. Overall, the
407 consistent prediction the bulk modulus in comparison of computational and experimental
408 data increases our confidence in the prediction of the elastic constants performed in this
409 work. The shear modulus and Poisson's ratio of $\gamma(U, Zr)$ were determined as well from the
410 lattice constants. The values for γ U were compared to the only experimental data sets
411 that were available. They were compared also to another data set for depleted γ U alloyed
412 with titanium. Due to the scarcity of experimental data on metallic fuel, it is important
413 to perform modernly designed experiments to provide data for validation of computational
414 work and computational codes.

415 The predicted sound velocity in $\gamma(U, Zr)$ tends to increase with Zr content. The decrease
416 of bulk modulus should lead to an increase in the sound velocity, however, the decrease in
417 the alloy density with Zr content has an inverse and competing effect on the sound velocity.
418 The results of our calculations show that the change in density has an overall dominant effect
419 leading to an overall increasing trend of the sound velocity with Zr content. The predicted
420 sound velocity showed a weak temperature dependence in this temperature range. The Debye
421 temperatures, which are calculated from the sound velocity data, showed similar behavior
422 to the sound velocity, as expected. This information can be incorporated into mesoscale and
423 engineering scale models which investigate the mechanical properties of $\gamma(U, Zr)$ and thermal
424 transport across the UZr-sodium bond through acoustic mismatch theory.

425 Acknowledgements

426 This work is supported through the INL Laboratory Directed Research and Development
427 (LDRD) Program under DOE Idaho Operations Office Contract DE-AC07-05ID14517. This

428 manuscript has been authored by Battelle Energy Alliance, LLC with the U.S. Department
 429 of Energy. The publisher, by accepting the article for publication, acknowledges that the
 430 U.S. Government retains a nonexclusive, paid-up, irrevocable, worldwide license to publish
 431 or reproduce the published form of this manuscript, or allow others to do so, for U.S. Govern-
 432 ment purposes. This research made use of the resources of the High-Performance Computing
 433 Center at Idaho National Laboratory, which is supported by the Office of Nuclear Energy of
 434 the U.S. Department of Energy and the Nuclear Science User Facilities.

435 **Appendix A. Tabulated data**

Table A.1: **The equilibrium lattice parameter of γ -(U, Zr) between 1000 K and 1400 K.**

<i>At.% Zr</i>	1000 K	1100 K	1200 K	1300 K	1400 K
0	3.490	3.495	3.500	3.505	3.510
7.0	3.503	3.508	3.512	3.517	3.521
14.0	3.515	3.519	3.523	3.528	3.532
18.8	3.523	3.527	3.531	3.535	3.540
22.7	3.528	3.533	3.537	3.540	3.544
26.6	3.534	3.538	3.542	3.546	3.550
32.0	3.542	3.546	3.549	3.553	3.557

Table A.2: **Elastic constants of γ -(U, Zr) as a function of temperature.**

0 at.% Zr	C ₁₁	C ₁₂	C ₄₄	22.6 at.% Zr	C ₁₁	C ₁₂	C ₄₄
1000 K	110.86	102.13	53.74	1000 K	106.79	75.78	54.57
1100 K	117.90	99.04	53.24	1100 K	106.65	75.69	49.41
1200 K	119.08	96.99	52.47	1200 K	103.57	75.15	47.51
1300 K	116.03	97.54	46.54	1300 K	103.99	70.64	45.06
1400 K	111.36	93.62	43.58	1400 K	99.56	71.33	44.09
7.0 at.% Zr	C ₁₁	C ₁₂	C ₄₄	26.6 at.% Zr	C ₁₁	C ₁₂	C ₄₄
1000 K	105.50	92.23	47.37	1000 K	116.40	76.65	48.54
1100 K	111.12	94.16	50.05	1100 K	111.08	77.45	50.19
1200 K	104.72	88.27	46.49	1200 K	115.56	77.24	48.41
1300 K	111.34	88.42	49.54	1300 K	110.42	76.08	48.74
1400 K	100.17	84.14	40.86	1400 K	106.18	75.13	45.19
14.0 at.% Zr	C ₁₁	C ₁₂	C ₄₄	32.0 at.% Zr	C ₁₁	C ₁₂	C ₄₄
1000 K	104.27	89.18	55.11	1000 K	107.71	72.82	48.39
1100 K	107.43	92.93	49.78	1100 K	104.41	75.24	47.55
1200 K	103.60	86.51	48.89	1200 K	100.72	70.09	48.48
1300 K	108.84	89.83	44.01	1300 K	94.46	72.53	46.85
1400 K	98.30	85.14	45.05	1400 K	98.02	69.68	45.22
18.8 at.% Zr	C ₁₁	C ₁₂	C ₄₄	100.00 at.% Zr	C ₁₁	C ₁₂	C ₄₄
1000 K	110.52	82.96	50.75	1000 K	83.78	76.14	54.50
1100 K	106.67	84.53	50.24	1100 K	83.73	72.85	54.19
1200 K	111.28	84.73	46.91	1200 K	83.24	73.09	50.67
1300 K	100.54	80.50	44.76	1300 K	84.74	71.61	51.17
1400 K	105.87	81.76	42.85	1400 K	83.21	72.54	54.20

436 **References**

- 437 [1] F. Habashi, Uranium, Physical and Chemical Properties, Springer New York, New York,
438 NY, 2013, pp. 2285–2287.
- 439 [2] P. Söderlind, Theory of the crystal structures of cerium and the light actinides, Adv. In
440 Phys. 47 (6) (1998) 959–998.
- 441 [3] J. R. Davis, Metal Handbook Desk Edition, 2nd Edition, ASM, 1998.
- 442 [4] J. Galloway, C. Unal, N. Carlson, D. Porter, S. Hayes, Modeling constituent redistri-
443 bution in u-pu-zr metallic fuel using the advanced fuel performance code bison, Nucl.
444 Eng. Des. 286 (2015) 1–17.
- 445 [5] C. Taylor, Evaluation of first-principles techniques for obtaining materials parameters
446 of alpha uranium and the (001) alpha uranium surface, Phys. Rev. B 77 (2008) 094119.
- 447 [6] B. Beeler, D. Chaitanya, M. Baskes, M. Okuniewski, First principles calculations of the
448 structure and elastic constants of α, β and γ uranium, J. Nucl. Mat. 433 (2013) 143–151.
- 449 [7] S. Shang, A. Saengdeejing, Z. Mei, D. Kim, H. Zhang, Y. Ganeshan, W. Y., Z. Liu,
450 First-principles calculations of pure elements: Equations of state and elastic stiffness
451 constants, Comput. Mater. Sci. 48 (2010) 813–826.
- 452 [8] B.-T. Wang, P. Zhang, H.-Y. Liu, W.-D. Li, P. Zhnag, First-principles calculations of
453 phase transition, elastic modulus, and superconductivity under pressure for zirconium,
454 J. Appl. Phys. 109 (2011) 063514.
- 455 [9] M. Mendeleev, G. Ackland, Development of an interatomic potential for the simulation
456 of phase transformations in zirconium, Philos. Mag. Lett. 87 (2007) 349–359.
- 457 [10] H. Ikehata, N. Nagasako, T. Furuta, A. Fukumoto, K. Miwa, T. Saito, First-principles
458 calculations for development of low elastic modulus ti alloys, Phys. REv. B. 70 (2004)
459 174113.
- 460 [11] R. Ahuja, J. Wills, B. Johansson, O. Eriksson, Crystal structures of ti, zr, and hf under
461 compression: Theory, Phys. REv. B. 48 (1993) 16269.
- 462 [12] I. Khalatnikov, Heat Exchange Between a Solid and Helium II, 1st Edition, Taylor &
463 Francis, 1965.
- 464 [13] G. L. POLLACK, Kapitza resistance, Rev. Mod. Phys. 41 (1969) 48–81.

- 465 [14] G. Dharmadurai, Acoustic mismatch theory for heat flow across fuel-cladding interfaces
466 in fast reactors, *Nuclear Science and Engineering* 84 (4) (1983) 345–349.
- 467 [15] D. E. Janney, S. L. Hayes, C. A. Adkins, A critical review of the experimentally known
468 properties of U-Pu-Zr alloys. part 1: Phases and phase diagrams, *Nuclear Technology*
469 205 (11) (2019) 1387–1415.
- 470 [16] A. Aly, B. Beeler, M. Avramova, Ab initio molecular dynamics investigation of γ -(u, zr)
471 structural and thermal properties as a function of temperature and composition, *J. Nucl.*
472 *Mater.* 561 (2022) 153523.
- 473 [17] B. Beeler, A. Casagrande, L. Aagesen, Y. Zhang, S. Novascone, Atomistic calculations
474 of the surface energy as a function of composition and temperature in γ U-Zr to inform
475 fuel performance modeling, *J. Nucl. Mater.* 540 (2020) 152271.
- 476 [18] J. W. Taylor, S. D. Ford, Solid metal-liquid metal interaction studies: Part ii contact
477 angle relationships for sodium on solids, AERE M/R 1729 (1955).
- 478 [19] G. Kresse, J. Hafner, Ab initio molecular dynamics for liquid metals, *Phys. Rev. B* 47
479 (1993) 558.
- 480 [20] G. Kresse, J. Furthmüller, Efficiency of ab-initio total energy calculations for metals and
481 semiconductors using a plane-wave basis set, *Comput. Mat. Sci.* 6 (1996) 15–50.
- 482 [21] P. Blochl, Projector augmented-wave method, *Phys. Rev. B* 50 (1994) 17953.
- 483 [22] J. Perdew, K. Burke, M. Ernzerhof, Generalized gradient approximation made simple,
484 *Phys. Rev. Lett.* 77 (1996) 3865–3868.
- 485 [23] H. Monkhorst, J. Pack, Special points for brillouin-zone integration, *Phys. Rev. B* 13
486 (1976) 5188.
- 487 [24] B. Beeler, D. Andersson, C. Jiang, Y. Zhang, Ab initio molecular dynamics investigation
488 of point defects in γ -U, *J. Nucl. Mater.* 545 (2021) 152714.
- 489 [25] G.-Y. Huang, B. Wirth, First-principles study of bubble nucleation and growth behav-
490 iors in alpha u-zr, *J. Phys.: Cond. Mat.* 24 (2012) 415404.
- 491 [26] B. Sadigh, A. Kutepov, A. Landa, P. Söderlind, Assessing relativistic effects and electron
492 correlation in the actinide metals Th to Pu, *Appl. Sci.* 9 (23) (2019).
- 493 [27] A. Stukowski, Visualization and analysis of atomistic simulation data with ovito – the
494 open visualization tool, *Modeling Simul. Mater. Sci. Eng.* 18 (2010) 015012.

- 495 [28] M. Hanfland, I. Loa, K. Syassen, Sodium under pressure: bcc to fcc structural transition
496 and pressure-volume relation to 100 gpa, *Phys. Rev. B* 65 (2002) 184109.
- 497 [29] C. S. Barrett, X-ray study of the alkali metals at low temperatures, *Acta Cryst.* 9 (1956)
498 671–677.
- 499 [30] K. Baral, A. Li, W.-Y. Ching, *Ab initio* molecular dynamics simulation of na-doped
500 aluminosilicate glasses and glass-water interaction, *AIP Adv.* 9 (2019) 075218.
- 501 [31] S. Ebnesajjad, A. H. Landrock, Chapter 2 - surface tension and its measurement, in:
502 *Adhesives Technology Handbook*, third edition Edition, William Andrew Publishing,
503 Boston, 2015, pp. 19–34.
- 504 [32] R. Hill, The elastic behaviour of a crystalline aggregate, *Proc. Phys. Soc. A* 65 (1952)
505 349.
- 506 [33] W. Voigt, *Lehrbuch der Kristallphysik*, 1st Edition, Vieweg+teubner Verlag, Germany,
507 1928.
- 508 [34] A. Reuss, Z. Agnew, Berechnung der fließgrenze von mischkristallen auf grund der
509 plastizitätsbedingung für einkristalle, *Math. Mech.* 9 (1929) 49–58.
- 510 [35] M. A. Ghebouli, B. Ghebouli, M. Fatmi, First-principles calculations on structural,
511 elastic, electronic, optical and thermal properties of CsPbCl_3 perovskite, *Phys. B* 406
512 (2011) 1837–1843.
- 513 [36] D. H. Chung, W. R. Buessem, The voigt-reuss-hill approximation and elastic moduli of
514 polycrystalline MgO , CaF_2 , $\beta\text{-ZnS}$, ZnSe , and CdTe , *J. Appl. Phys.* 38 (1967) 2535.
- 515 [37] J. Toonder, J. Dommelen, F. Baaijens, The relation between single crystal elasticity
516 and the effective elastic behaviour of polycrystalline materials: theory, measurement
517 and computation, *Modelling Simul. Mater. Sci. Eng.* 7 (1999) 909–928.
- 518 [38] O. L. Anderson, A simplified method for calculating the debye temperature from elastic
519 constants, *J. Phys. Chem. Solids* 24 (1963) 909–917.
- 520 [39] A. G. MALONDA, A. G. CARLES, 7 - radioactivity counting statistics, in: *Handbook*
521 *of Radioactivity Analysis*, second edition Edition, Academic Press, San Diego, 2003,
522 pp. 609–654.
- 523 [40] L. Leibowitz, M. Chasanov, R. Blomquist, Speed of sound in liquid sodium to 1000°C,
524 *J. Appl. Phys.* 42 (1971) 2135.

- 525 [41] J. P. Stone, C. T. Ewing, J. R. Spann, E. W. Steinkuller, D. D. Williams, R. R. Miller,
526 High temperature pvt properties of sodium, potassium, and cesium, *J. Chem. Eng.*
527 11 (3) (1966) 309–314.
- 528 [42] T. Iida, R. I. L. GuthrieDavis, *The Physical Properties of Liquid Metals*, Clarendon
529 press. Oxford, 1988.
- 530 [43] J. H. Goldman, Surface tension of sodium, *J. Nucl. Mater.* 126 (1984) 86–88.
- 531 [44] J. K. Fink, L. Leibowitz, Thermophysical properties of sodium, ANL-CEN-RSD-79-1,
532 Argonne National Laboratory Report, Illinois, USA, 1979.
- 533 [45] M. Pozzo, M. P. Desjarlais, D. Alfe, Electrical and thermal conductivity of liquid sodium
534 from first-principles calculations, *Phys. Rev. B* 84 (2011) 054203.
- 535 [46] A. Bengtson, H. O. Nam, S. Saha, R. Sakidja, D. Morgan, First-principles molecular
536 dynamics modeling of the licl–kcl molten salt system, *Computational Materials Science*
537 83 (2014) 362–370.
- 538 [47] J. Song, X. Li, S. Shi, L. Yan, T. Jiang, S. Peng, Towards the calculations of redox poten-
539 tials in molten licl-kcl eutectic by ensemble averages based on first principles molecular
540 dynamics, *Electrochimica Acta* 248 (2017) 462–469.
- 541 [48] K. Duemmler, Y. Lin, M. Woods, T. Karlsson, R. Gakhar, B. Beeler, Evaluation of
542 thermophysical properties of the licl-kcl system via ab initio and experimental methods,
543 *J. Nucl. Mater.* 559 (2022) 153414.
- 544 [49] N. Eustathopoulos, B. Drevet, E. Ricci, Temperature coefficient of surface tension for
545 pure liquid metals, *Journal of Crystal Growth* 191 (1) (1998) 268–274.
- 546 [50] E. N. Hodkin, D. A. Mortimer, M. G. Nicholas, D. M. Poole, The surface and interfacial
547 energies of the uranium-uranium carbide system, *J. Nucl. Mater.* 39 (1971) 59–68.
- 548 [51] G. Hu, C. Luo, L. Wu, Q. Tang, R. Z., B. Xu, Molecular dynamics simulation of
549 solid/liquid interfacial energy of uranium, *J. Nucl. Mater.* 538 (2020) 152183.
- 550 [52] A. P. Moore, B. Beeler, M. Baskes, M. Okuniewski, C. S. Deo, Atomistic ordering in
551 body centered cubic uranium-zirconium alloy, *MRS Proceedings* 1514 (2013) 27–35.
- 552 [53] A. P. Moore, B. Beeler, C. Deo, M. I. Baskes, M. A. Okuniewski, Atomistic modeling
553 of high temperature uranium-zirconium alloy structure and thermodynamics, *J. Nucl.*
554 *Mat.* 467 (2015) 802–819.

- 555 [54] J. H. Li, Q. B. Ren, C. H. Lu, L. Lu, Y. Dai, B. X. Liu, Structure, formation energies
556 and elastic constants of uranium metal investigated by first principles calculations, J.
557 Alloys Compd. 516 (2012) 139–143.
- 558 [55] C.-S. Yoo, H. Cyun, P. Söderlind, Phase diagram of uranium t high pressure and tem-
559 peratures, Phys. Rev. B 57 (1998) 10359.
- 560 [56] Y. Zhao, J. Zhang, C. Pantea, J. Qian, L. Daemen, et al., Thermal equations of state
561 of the α , β , and ω phases of zirconium, Phys. Rev. B 71 (2005) 184119.
- 562 [57] P. E. Armstrong, D. T. Eash, J. E. Hockett, Elastic moduli of alpha, beta and gamma
563 polycrystalline uranium, J. Nucl. Mater. 45 (1972) 211–216.
- 564 [58] A. D. Schwope, G. T. Muehlenkamp, Unpublished, reported in A.N. Holden, Physical
565 Metallurgy of Uranium (1958) 61.
- 566 [59] K. H. Keene, J. T. Hartman JR., A. Wolfenden, L. G. M., Determination of dynamic
567 young’s modlulus, shear modulus, and poissson’s ratio as a function of temperature
568 for depleted uranium-0.75 *wt%* titanium using the piezoelectric ultrasonic composite
569 oscillator technique, J. Nucl. Mater. 149 (1987) 218–226.